applied sciences

MDPI

*Article*

# Removal of Metals and Dyes in Water Using Low-Cost Agro-Industrial Waste Materials

**Candelaria Tejada-Tovar [1], Ángel Villabona-Ortíz [1] and Rodrigo Ortega-Toro [2,*]**

[1] Process Design, and Biomass Utilization Research Group (IDAB), Chemical Engineering Department, Universidad de Cartagena, Avenida del Consulado St. 30, Cartagena de Indias 130015, Colombia; ctejadat@unicartagena.edu.co (C.T.-T.); avillabonao@unicartagena.edu.co (Á.V.-O.)

[2] Food Packaging and Shelf-Life Research Group (FP&SL), Food Engineering Department, Universidad de Cartagena, Avenida del Consulado St. 30, Cartagena de Indias 130015, Colombia

* Correspondence: rortegap1@unicartagena.edu.co

**Abstract:** The pollution of water bodies due to the discharge of effluents without treatment is a global problem. Therefore, different technologies have been implemented for the removal of contaminants from wastewater before the final disposition. Among them, adsorption processes using residual biomasses are becoming very popular due to the low cost and high availability of adsorbents. Thus, in the present work, the synthesis of modified biochar from agro-industrial residues derived from the wheat-processing industry, as a valorization alternative of these residues, for its use in the removal of Cr (VI) and methylene blue (MB) has been analyzed. The biochar was prepared using a ramp function of 5 °C/min until 250 °C for 30 min. The adsorption tests were developed in a batch system, using 30 mg of adsorbent in 10 mL of solution. From SEM analysis, the formation of tubular cavities and porous structure was seen, caused by the basic hydrolysis with KOH. From adsorption tests, an adsorption capacity of 12.98 mg/g and 97.38% of efficiency for MB at pH 10 was noted, while for Cr (VI), it was 11.35 mg/g and 85.15% at pH 2. Freundlich's model adjusted the adsorption equilibrium data with $R^2 > 0.9$. The maximum adsorption capacities in the monolayer were 186,375 mg/g and 90.723 mg/g for Cr (VI) and MB, according to Langmuir's model. From a kinetic study, it can be said that the process occurs by chemisorption through electrostatic interaction and ionic interchange between adsorbate and adsorbent.

**Keywords:** equilibrium; Langmuir; adsorption capacity; wastewater treatment

check for updates

**Citation:** Tejada-Tovar, C.; Villabona-Ortíz, Á.; Ortega-Toro, R. Removal of Metals and Dyes in Water Using Low-Cost Agro-Industrial Waste Materials. *Appl. Sci.* **2023**, *13*, 8481. https://doi.org/10.3390/app13148481

Academic Editors: Wojciech Janczukowicz and Joanna Rodziewicz

Received: 21 June 2023
Revised: 14 July 2023
Accepted: 17 July 2023
Published: 22 July 2023

**Copyright:** © 2023 by the authors. Licensee MDPI, Basel, Switzerland. This article is an open access article distributed under the terms and conditions of the Creative Commons Attribution (CC BY) license (https://creativecommons.org/licenses/by/4.0/).

## 1. Introduction

Pollution of water resources due to the effect of organic and inorganic compounds is rising proportionally with the augmenting of the global population and anthropogenic activities [1]. Dyes are widely used as colorants in industries such as pharmaceutical, food, printing, leather, and textile, among others [2]. A total of 700,000 dyes are used commercially, and around 10% of the dyes used in different sectors are discharged in effluents without proper treatment [1]. The discharge of untreated tinted wastewater into water bodies can cause environmental damage, i.e., oxygen content reduction and diminished sunlight penetration, which puts the life of aquatic animals and plants in danger [3]. Among dyes, MB is a cationic dye, has a heterocyclic aromatic structure, and has high volume production because it is extensively applied in coloring paper, hair colorant, dyeing cotton, wool, and paper stock coating [4], among others. Because of its side effects on human health, it has relevance as a pollutant in water systems.

Heavy metals are persistent, non-biodegradable, bioaccumulative, and toxic. Among them, chromium is listed in the top 20 contaminants under the category of hazardous materials. It is extensively used in industrial processes such as fertilizer, electroplating, leather tanning, and paint, among others. Chromium commonly exists in nature as Cr (III) and Cr (VI), the first being relatively harmless, whereas Cr (VI) is considered carcinogenic

due to its strong oxidizing properties. In humans, it can cause dermatitis, hemorrhage, bronchitis, lung cancer, and liver inflammation [5]. The maximum permissible levels of Cr (VI) in industrial effluent and potable water are 0.25 and 0.05 mg/L, respectively [6].

Consequently, there is statistical data showing that approximately two million tons of residual effluents are discharged into natural water basins, of which 33% correspond to untreated industrial discharges, affecting 90% of water supply drinking water [7]. A clear example of this pollution comes from the textile industries, the most significant contaminant being organic dyes, generating 54% of the pollution worldwide, followed by the dry cleaning industry with 21%, the paper and pulp industry with 10%, and the painting industry with 8% of effluents contaminated by dyes [8]. In addition, the contamination by chromium present in industrial effluents belongs to 3970 mg/kg in wastewater from the mining industry, 794 mg/kg from the chrome industry, and 2915 mg/kg from the steel industry [9]. These high chromium concentrations in wastewater exceed those that the World Health Organization allows, establishing a permissible limit in industrial discharges of 2 mg/L [10].

Considering the above, the treatment of polluted effluents before their discharge into water bodies is necessary. Among the technologies used in the removal of contaminants from water, adsorption is widely used due to its simplicity, easy operation, efficiency, insensitivity to toxic contaminants, and selectivity towards pollutants, even at low concentrations [11]. The use of activated carbon is common in adsorption systems because it exhibits characteristic features of higher surface area, porous structure, variable surface chemistry properties, and higher mechanical strength. Nevertheless, commercial activated carbons are produced using coal, which is not an economical or non-renewable material [12]. Considering the above, the synthesis of activated carbon from cheap and efficient precursors such as agricultural wastes, low-grade plants, forest residues, and industrial by-products is being studied.

Recent studies have used agro-industrial residues as an ecological and sustainable strategy for manufacturing biochar with adsorption capacity for heavy metals and cationic dyes such as chromium and methylene blue (MB). Khalil et al. [13] studied the preparation of carbons from rice husks and tea residues for their application in Cr (VI) removal processes. It is worth noting that the biomaterials obtained 99.3% and 96.8% metal removal, respectively, the former being the most efficient. Likewise, Shakya and Agarwal [14] evaluated the biomass of pineapple peels in slow pyrolysis processes at different temperatures and its application in removing Cr (VI). The carbon prepared at a temperature of 350 °C obtained the best adsorption capacity of 41.67 mg/g, in comparison with the others, and the chemical adsorption with covalent interactions between the metal ions and the functional groups of the surface of the biomaterial, as the most relevant removal mechanism in the process.

On the other hand, Al-Mokhalelati et al. [15] carried out studies on the adsorption capacity of sugarcane bagasse treated with potassium hydroxide (KOH) to remove MB. The study of the process was carried out as a batch, analyzing variables such as contact time, pH, adsorbent dose, and the initial concentration of the solution, the presence of a large number of characteristic functional groups of this type of lignocellulosic materials, such as the -OH, C-H group, and the C=O carbonyl group. In addition, the spectrum results obtained after adsorption established that the adsorption occurred largely thanks to these functional groups. Regarding the adsorption studies, the optimal variables of the process were found to be 0.1 g of dose, an equilibrium time of 1.5 h, a pH range between 5 and 9, and the initial concentration of methylene blue of 100 ppm. Finally, the maximum adsorption capacities obtained were 186.67 mg/g for the untreated bagasse and 195.44 mg/g for the bagasse treated with KOH. With this, the importance of implementing modifications in the lignocellulosic biomass treatment processes that will be applied to remove contaminants such as Cr (VI) and MB is denoted.

Thus, the present study is dedicated to using wheat bran as raw material for the synthesis of biochar for its use in the removal of methylene blue and hexavalent chromium

from aqueous solutions. The adsorbents were characterized using Fourier transform infrared spectroscopy (FT-IR), scanning electron microscopy (SEM), pH point of zero charge, and Boehm titration. The parameters of the adsorption system were optimized to attain the maximum removal efficiency of methylene blue and hexavalent chromium. The adsorption process mechanisms were examined by fitting the experimental data to isotherms and kinetic models.

## 2. Materials and Methods

### *2.1. Materials and Reagents*

The potassium hydroxide (KOH), sodium hydroxide (NaOH), potassium dichromate ($K_2Cr_2O_7$), acetone ($C_3H_6O$), 1,5-difenilcarbazide ($C_{13}H_{14}N_4O$), hydrochloric acid (HCl), phosphoric acid ($H_3PO_4$), sodium carbonate ($Na_2CO_3$), sodium bicarbonate ($NaHCO_3$), and MB ($C_{16}H_{18}ClN_3S$) are analytical grade by Merck. All the experiments were done with distilled water. A digital pH meter HI 9814, Hanna (Woonsocket, RI, USA) was used.

### *2.2. Modified Biochar Synthesis*

Wheat bran was used as raw biomass for the synthesis of the biochar activated with KOH (MWBC). This material was supplied already pre-treated by a company in the flour sector located in the city of Bogotá, Colombia; therefore, it was ready to be heat treated. The WB was heated in a muffle with a ramp function of 5 °C/min until 250 °C [16], and it was maintained for 30 min. Then, the material was left to cool, obtaining the unmodified biochar (WBC) (Figure 1). For the modification of the WBC by means of basic hydrolysis, 20 g were put in contact with 200 mL of KOH 3 M; the mixture was stirred in a Cimarec, Thermo Scientific (Waltham, MA, USA) for an hour at 60–70 °C. Then, the MWBC was washed until neutral pH. The material was dried at 80 °C for 12 h and reserved for use in the adsorption processes [17]. The choice of KOH is justifiable thanks to its wide use in biochar modification due to its alkaline properties and ability to activate and improve the adsorption characteristics of the material [18]. Furthermore, KOH effectively increases the porosity and specific surface area of biochar, which improves its adsorption capacity [19].

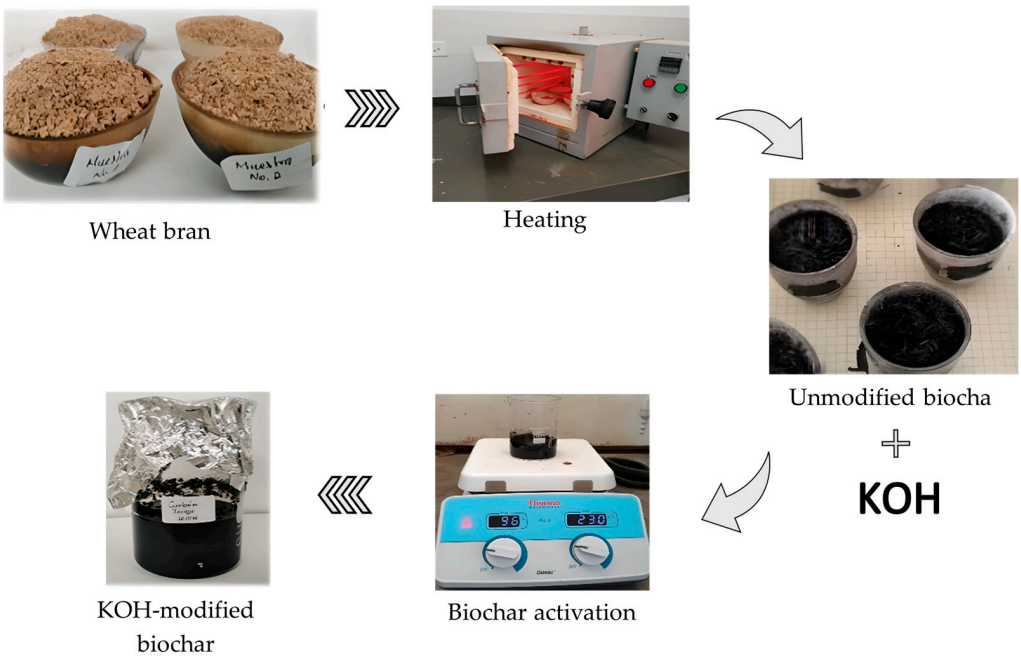



**Figure 1.** Methodology for the preparation and activation of biochar from wheat bran.

### 2.3. Characterization Methods

Scanning electron microscopy (SEM) was used to determine the surface characteristics of the MWBC. The functional groups were determined by Fourier transform infrared spectroscopy (FTIR) before and after the adsorption process of Cr (VI) and MB.

For the quantification of the functional groups, the Boehm titration was used; for this, 1.5 g of MWBC was put in 50 mL of solutions 0.5 M of $NaHCO_3$, $Na_2CO_3$, and NaOH. The samples were stirred for 24 h and were filtered. An aliquot of 10 mL was taken for the acidification with HCl 0.05 M, ensuring a complete neutralization of the base. The acidified solutions were titrated with 0.05 M NaOH. A pH meter was used to determine the final point at pH 7 [20]. The quantities of the groups present in the MWBC were determined by Equation (1):

$$n_{CSF} = \frac{n_{HCl}}{n_B}[B]V_B - ([HCl]V_{HCl} - [NaOH]V_{NaOH})\frac{V_B}{V_a} \quad (1)$$

where $n_{CSF}$ is the molar quantity of functional groups [mol]; $n_{HCl}$ is the number of moles of HCl [mol], $n_B$ is the number of mol of the base [mol], $[B]$ is the concentration of the base [mol/L], $V_B$ is the volume of the base [L], $[HCl]$ is the concentration of HCl [mol/L], $V_{HCl}$ is the volume of HCl used in the acidification of the base [L], $[NaOH]$ is the concentration of NaOH [mol/L], $V_{NaOH}$ is the volume of NaOH used in the titration [L], and $V_a$ is the volume of the aliquot taken [L].

The pH point of zero charge ($pH_{PZC}$) was determined to establish the equilibrium charge of the adsorbent surface. Therefore, water samples with pH between 3 and 11 were put in contact with 50 mg of MWBC and stirred for 24 h at room temperature. The final pH of each sample was taken to be analyzed by graphic method and identify the $pH_{PZC}$ of the material [21].

### 2.4. Adsorption Assays

The MB adsorption assays were performed following the ASTM C1777-20 [22]. The effect of the pH from 7 to 11 was evaluated by employing a 40 mg/L MB solution in contact with 30 mg of adsorbent in 10 mL of solution, considering the cationic nature of the pollutant. The pH of the solutions was adjusted using NaOH and HCl 0.1 M [23]. In addition, the effect of the initial concentration (10, 20, 40, 60, 80, and 100 mg/L) by adsorption assays in the batch system during 24 h in an orbital shaker HS-120460, Heathrow Scientific (Vernon Hills, IL, USA) [24]. The final concentration was determined by UV-Vis at 664 nm [22].

On the other hand, the adsorption tests of Cr (VI) were done by following the ASTM D1687-17. The effect of the pH from 2 to 7 was done using a 100 mg/L solution of Cr (VI), considering that at acid pH, the chromium remover was better [25]. The effect of the initial concentration was analyzed (5, 10, 15, 20, 30, 40, 50, 75, 100, 150, 200, 250, and 300 mg/L) by putting 30 mg of adsorbent in contact with 10 mL of solution during 24 h. The residual concentration of Cr (VI) was determined by the photo-colorimetric method of the difenilcarbazide, using an UV-Vis at 540 nm [26].

All the experiments were done by duplicate at room conditions and a stirring rate of 200 rpm. The efficiency of the removal (RE) was determined by Equation (2), and the adsorption capacity by Equation (3).

$$RE[\%] = \frac{C_i - C_e}{C_i} \times 100 \quad (2)$$

$$q_e[mg/g] = \frac{(C_i - C_e) \times V}{M} \quad (3)$$

where $RE$ is the pollutant removal percentage, $q_e$ is the adsorbent adsorption capacity [mg/g], $C_i$ y $C_e$ is the initial and equilibrium concentration, respectively, [mg/L], $V$ is the volume of solution [L], and $M$ is the amount of adsorbent [g].

### 2.5. Adsorption Isotherms

The adsorption isotherms describe the interaction between adsorbate and adsorbent in the equilibrium. In accordance with the interaction between the surface of the material, the adsorbate particles, and the nature of the process, the results can be described by established models for determining the adsorption mechanism and measuring the adsorption capacity of any adsorbent [27]. The equilibrium of adsorption was studied by varying the initial concentration of MB (10, 20, 40, 60, 80, and 100 mg/L) and Cr (VI) (5, 10, 15, 20, 30, 40, 50, 75, 100, 150, 200, 250, and 300 mg/L) and using 30 mg of adsorbent at room conditions and 200 rpm for 24 h. The experimental data were adjusted to the models of Langmuir and Freundlich.

Langmuir's model (Equation (4)) describes monolayer adsorption based on specific homogeneous sites in the adsorbent's surface, forming a single surface layer [28].

$$q_e = \frac{q_{max}^L k_L C_e}{1 + k_L C_e} \tag{4}$$

where $C_e$ is the remaining concentration of pollutant in the equilibrium [mg/L], $q_e$ is the amount of pollutant adsorbed in the equilibrium [mg/g], $q_{max}^L$ is the maximum adsorption capacity of Langmuir's model in the equilibrium [mg/g], and $k_L$ is Langmuir's constant associated with the affinity of the adsorbent for the pollutant [L/mg]. Freundlich's model (Equation (5)) is based on monolayer adsorption but considers the heterogeneity of the active sites with different activation energies for the adsorption process [29].

$$q_e = K_F C_e^{1/n} \tag{5}$$

where $K_F$ and $n$ are constants of the model.

### 2.6. Adsorption Kinetics

The kinetic experiments were done at the best experimental conditions of pH and adsorbent dose. A total of 30 mg in 10 mL was used as the adsorbent dose for all systems. All assays were stirred at 200 rpm taking samples in a range of 5 to 420 min and taking a last date at 24 h. The kinetic data indicate the duration necessary to achieve the equilibrium condition [30]. Therefore, the models of Lagergren of pseudo-first order (Equation (6)), pseudo-second order (Equation (7)), and Elovich (Equation (8)) were used for analyzing the kinetic experimental data.

Lagergren's or the pseudo-first-order model explains the relation between the occupation rate of active adsorption sites of the adsorbents and the number of vacant sites [31].

$$q_t = q_e\left(1 - e^{-K_1 t}\right) \tag{6}$$

where $q_t$ is the adsorption capacity at a time $t$ [mg/g], $q_e$ is the adsorption capacity at the equilibrium [mg/g], $K_1$ is the adsorption rate constant [$min^{-1}$], and $t$ is the contact time [min]. The model of the pseudo-second order explains the Ho model or the pseudo-second order explains dependence on adsorption capacity over time [31,32]:

$$q_t = \frac{q_e^2 K_2 t}{1 + q_e^2 K_2 t} \tag{7}$$

where $K_2$ is the second-order adsorption rate constant [g/mg/min], and $t$ is the time of contact [min]. Elovich's model establishes that the activation energy augments with the adsorption time, and the adsorbent surface is heterogeneous; furthermore, it allows the modeling of the chemisorption of the fluid in the solid [32].

$$q_t = \frac{lnln\ (1 + \alpha\beta t)}{\beta} \tag{8}$$

where $\alpha$ and $\beta$ are the adjusting parameters of Elovich's model.

### 2.7. Competitive Adsorption Tests

The multicomponent adsorption tests were done at room conditions. The binary experiments were carried out under the same conditions of temperature, amount of adsorbent, agitation, and pH as the individual adsorption; thus, the concentration of one of the pollutants was fixed, while the amount of the interfering pollutant was varied to determine the effect on the adsorption of the first one. Interference tests were carried out for the Cr (VI)-MB system. The concentrations studied are shown in Table 1, where the response variable in each trial was adsorbent capacity ($q_e$).

**Table 1.** Experimental conditions for multicomponent assays.

| | | | | | | |
|---|---|---|---|---|---|---|
| Cr (VI) isotherms | MB concentration, mg/L | 100 | | | | |
| | Cr (VI) concentration, mg/L | 3 | 7 | 10 | 13 | 16 |
| MB isotherms | Cr (VI) concentration, mg/L | 100 | | | | |
| | MB concentration, mg/L | 20 | 40 | 60 | 80 | 100 |

## 3. Results and Discussion

### 3.1. Characterization of the Biosorbent

Figure 2A shows the SEM analysis of the unmodified wheat bran biochar (WBC), and Figure 2B shows the KOH-modified biochar (MWBC). Figure 2A presents a rather rough laminar morphology with small lines that may be characteristic of the different elements found in a lignocellulosic material such as wheat; among them, Mg, K, P, S, N, O, and C can be found as the most predominant in the coal structure thanks to the thermal process to which they were subjected (Table 1). Regarding Figure 2B, the effects of basic hydrolysis are observed when the biochar is impregnated with KOH. The surface evidences tubular-type cavities characteristic of cellulose-based materials; also, its porous structure denotes a greater surface area and traits that can be used in adsorption processes [17,33]. In accordance with the energy-dispersive X-ray spectroscopy, the elements with the highest presence in the structure of the MWBC are carbon (59.87% w), oxygen (24.89% w), and potassium (15.25% w), confirming the successful modification process with KOH [17].

Considering the physical properties and the elemental content shown in Table 2, the modified biochar changes after alkali treatment. In particular, the KOH-modified wheat biochar shows a porous structure that denotes a higher specific surface area. This fact is also related to the fact that the basic hydrolysis effect helps to eliminate the inorganic matter present in the biochar during the activation process, which is reflected in the reduction of elements such as sulfur (S), phosphorus (P), nitrogen (N), and magnesium (Mg) [17].

Figure 3 presents the results of the determination of $pH_{PZC}$ for MWBC. This study is meaningful since the electric charges of sorbent materials will depend on the pH of the solution, which relates to the ionization of polar functional groups on the surface of the sorbent [34,35]. The MWBC exhibits a $pH_{PZC}$ of 9.25, which implies that at this value concerning the conditions of the environment, the surface load density of the adsorbent would be zero [36]. Solutions with pH lower than pHPZC will enhance the adsorption of anionic species by electrostatic interaction, and when pH > pHPZC, it will favor the adsorption of cationic compounds by covalent interactions [37].

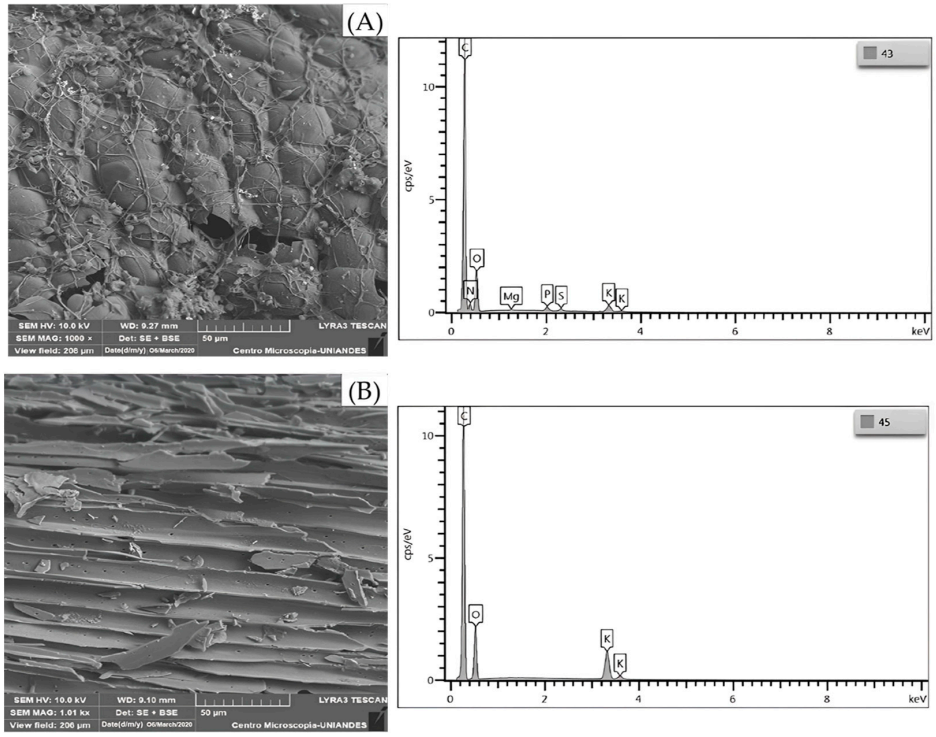



**Figure 2.** SEM-EDS analysis of the prepared biochar. (**A**) WBC and (**B**) MWBC.

**Table 2.** EDS analysis of coals prepared from wheat residues.

| Component | Unmodified Biochar (Wt.%) | Biochar Modified with KOH (Wt.%) |
|---|---|---|
| C | 64.11 | 59.87 |
| O | 19.48 | 24.89 |
| S | 0.71 | - |
| K | 3.46 | 15.25 |
| P | 1.01 | - |
| N | 10.99 | - |
| Mg | 0.24 | - |

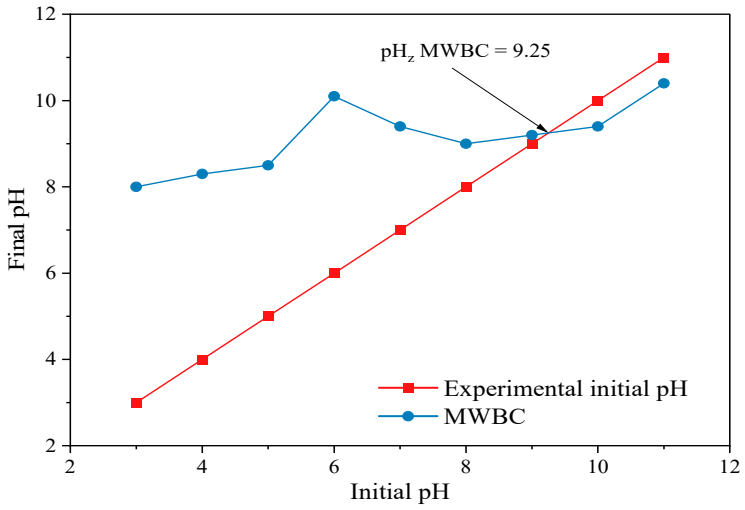



**Figure 3.** pH point of zero charge for WMBC.

From the FTIR analysis of MWBC before the adsorption process (Figure 4a), a peak is observed at 3122.36 $cm^{-1}$ caused by the asymmetric stretching of the -$NH_3$ group. The deformation of the -NH group present in secondary amides is observed at 1556.85 $cm^{-1}$. A strong asymmetric stretching is noticed in 1360.16 $cm^{-1}$ due to the -COO- present in carboxylic acid salts [38].

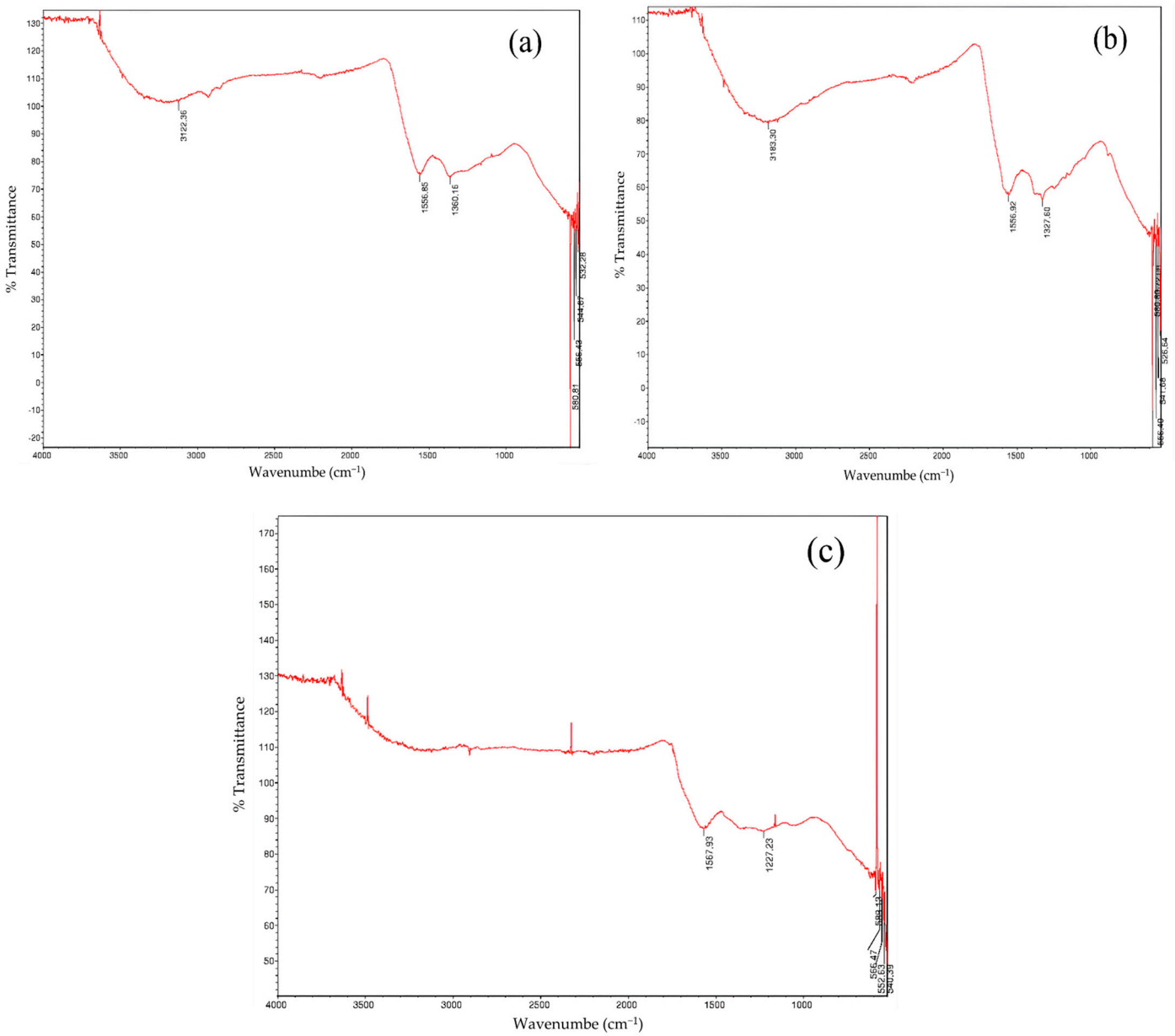



**Figure 4.** FTIR spectra for MWBC before (**a**) and after the adsorption of MB (**b**) and Cr (VI) (**c**).

The FTIR of the MWBC after MB adsorption (Figure 4b) shows an absorbance peak in 3183.30 $cm^{-1}$ because of the strong symmetric stretching -$NH_2$ and primary amides. Also, in 1556.92 $cm^{-1}$, the strong deformation of -NH is found, and the strong symmetric stretching in 1327.60 $cm^{-1}$ is caused by the presence of -$NO_2$ and -COO-, showing nitro aromatic compounds and carboxylic acid salts, respectively. Comparing the spectrum after MB adsorption with the clean MWBC is evidenced by the increase of the band corresponding to -$NH_3$, by effects of the MB presence in the surface structure of the material, considering this dye has nitrogen compounds in its cyclical aromatic structure, which interferes with the adsorption process [39].

After the adsorption of Cr (VI) (Figure 4c), there is a disturbance in 1567.93 $cm^{-1}$, which is caused by the strong symmetric stretching of -COO- y -$NO_2$ by effects of nitro aliphatic compounds and carboxylic acid salts, respectively. The strong band in 1227.23 $cm^{-1}$ is caused by the strong flexion of the -C-C-N group present in the amines [40,41]. The spectra after Cr (VI) adsorption show a low diminution of the band around carboxylic acid salts, denoting that they have enough relevance in Cr (VI) adsorption [42].

Table 3 shows the results of Boehm titration, presenting the density of functional groups by area unit, i.e., molecules by square nanometer. In addition, Figure 5 shows the behavior of the pH with respect to the amount of titrant species using different bases. The presence of carboxylic superficial groups denotes a high negative load in the material, which is quite related to attracting MB and CR (VI) molecules for being cationic species, which improves adsorption processes [43].

**Table 3.** Quantity of surface groups present in the MWBC material, determined by Boehm titration.

| Carboxylic, μ mol | Lactonic, μ mol | Phenolic, μ mol |
|---|---|---|
| 2175 | −630 | 495 |

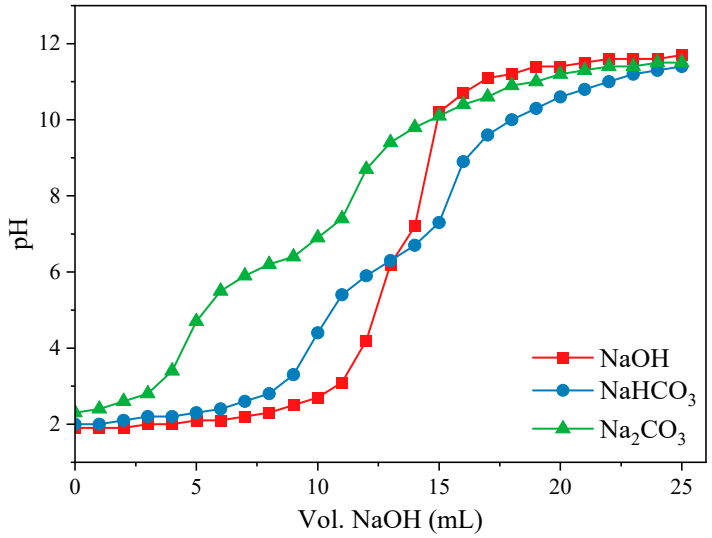



**Figure 5.** pH behavior during the MWBC titration.

### *3.2. Adsorption Parameters Effect*

#### 3.2.1. Effect of the pH

Adsorption processes are highly dependent on the pH of the solution because this variable affects the existent form of the compounds, the surface chemical properties of the adsorbent, the ionization grade of the adsorbent, and the affinity of the adsorbate in the function of the physical state of both materials [44,45].

Figure 6 shows that the removal efficiency of MB increases proportionally with the pH increasing. Thus, considering the alkaline nature of the KOH used as an activating agent, the above causes low competence between the hydrogen ions, which potentiates the increase of the negative charge on the surface of the adsorbent between the carbon and dye molecules, which consecutively alters the -COOH and -OH groups in their charge and electrical quantity, generating at the molecular level a process of electrostatic attraction, making the methylene blue adhere more easily to the adsorbent thanks to its cationic nature [23]. The highest removal and adsorption capacity occurs at pH 10, reaching 98.94% y 11.30 mg/g, respectively. It is important to consider that the pH of the solution influences the surface charge of methylene blue and biochar. The relatively lower adsorption capacity at pH 9 is because there may be a higher concentration of hydrogen ions (H+) in the

solution, which may compete with methylene blue for adsorption on the biochar. This ionic competition could limit the adsorption capacity of the dye, resulting in a lower observed removal efficiency. In addition, changes in the electrical charge of the functional groups on the biochar surface at pH 9 could affect the electrostatic attraction capacity between methylene blue and the adsorbent. The -COOH and -OH groups in the biochar could undergo modifications in their charge and electrical quantity, which alters the adsorption affinity of the dye compared to other pH values.

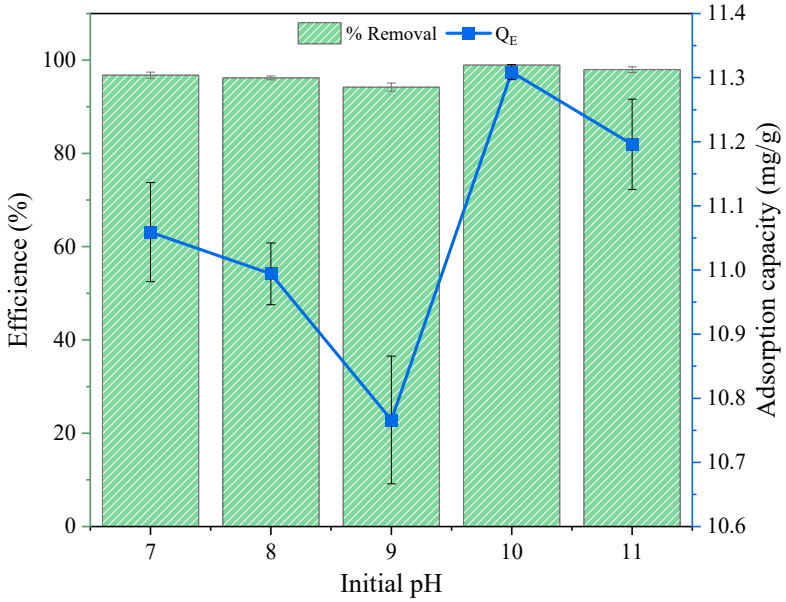



**Figure 6.** Effect of the pH onto MB adsorption at room conditions and 200 rpm.

Regarding Cr (VI) adsorption, in Figure 7 it is evidenced that the diminution of the pH caused an increase in the removal efficiency and adsorption capacity, achieving 79.35% y 26.45 mg/g, respectively. The results obtained in the present study are congruent with those reported in the literature, taking into account that, at low pH, the Cr (VI) is presented as $Cr_2O_7^{2-}$ y $HCrO_4^-$ in water solution, involving a combination with the active site of protonation by electrostatic adsorption [46]. Working at acidic pH allows the surface of the carbon to be positively charged, facilitating the adsorption of forms of Cr (VI) negatively charged [47–49]. In addition, at low pH, there are large amounts of $H^+$ ions in the bulk of the solution, leading to a process of protonation of the carbon surface, forming more positively charged sites and increasing the electrostatic attraction between the adsorbent and Cr (VI) [14,37,50]. Furthermore, at pH > 2, a low adsorption performance is presented, caused by the electrostatic repulsion of the anionic Cr (VI) and the KOH-modified wheat carbon, which originally has negative charges given its $pH_{PZC}$ of 9.25 [33].

### 3.2.2. Effect of the Adsorbent Dose

The adsorbent dose effect study was performed for MB adsorption, which functioned as a reference to determine the best dose and use it in Cr (VI) adsorption tests. Analyzing this parameter, it is considered that the greater the amount of adsorbent, the greater the number of active sites, which favors the adsorption process. This explanation is also valid when the surface area of the adsorbent is increased, or the particle size of the solid is reduced [28]. The effect of the dosage allows us to evaluate the adsorption capacity of a dye such as MB when working with less amount of adsorbent; this allows us to recognize the capacity of a dye from an economic point of view [45].

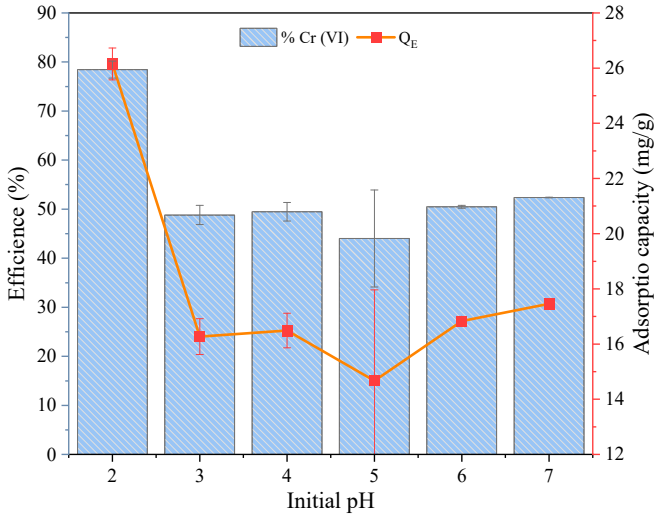



**Figure 7.** Effect of pH onto Cr (VI) adsorption at room conditions and 200 rpm.

Figure 8 shows a proportional behavior between the adsorbent amount and the removal efficiency of MB. On the other hand, an increase in the adsorbent dose causes the diminution of the adsorption capacity, which implies that the active sites present in the carbon are occupied to a great extent by the pollutant molecules; however, the higher the dose, the greater the number of active sites, denoting the presence of free active sites upon reaching equilibrium and obtaining a lower adsorption capacity. Regarding the effect of the initial concentration, the higher the concentration, the greater the adsorption capacity obtained, as in the case of 10 mg, but at 30 mg, the higher the concentration, the lower the adsorption capacity since active sites remain free to occupy. The same behavior is observed for the Cr (VI) removal process in Figure 9.

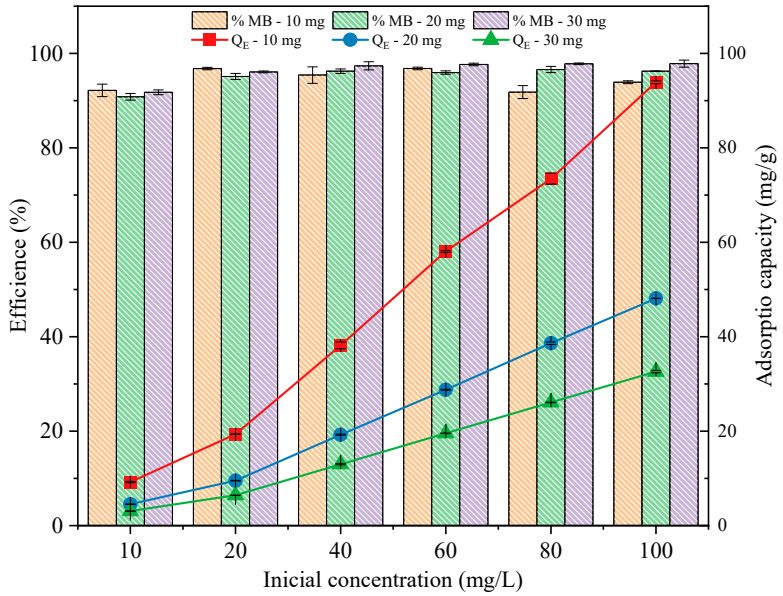



**Figure 8.** Effect of the adsorbent dose and initial concentration over the MB adsorption using MWBC.

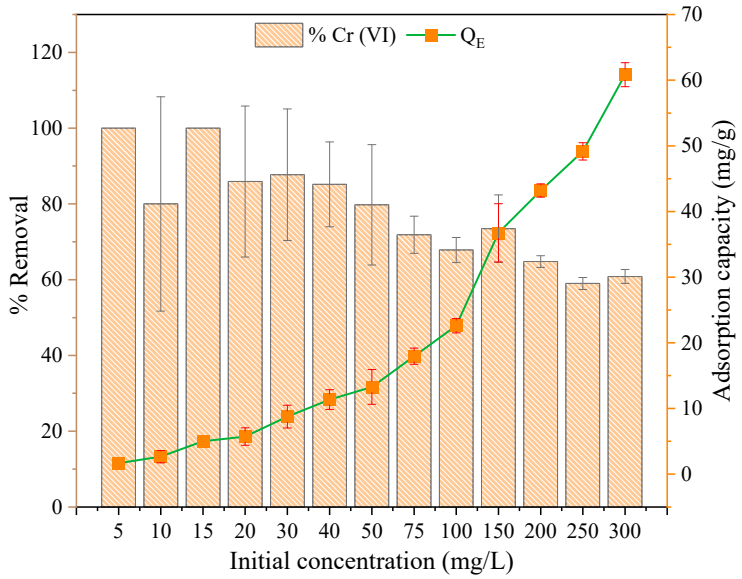



**Figure 9.** Effect of the initial concentration onto Cr (VI) adsorption using MWBC.

### *3.3. Adsorption Kinetic and Isotherm*

From Figure 10A and Table 4, it is observed that the experimental equilibrium adsorption data of MB are adjusted by Freundlich's model, indicating that the adsorbent surface is heterogeneous with many unequal active sites and different adsorption energies. Regarding Cr (VI) (Figure 10B), it can be said that the process is described by Langmuir's isotherm, denoting that at equilibrium, monolayer sorption of the solute occurs at a fixed number of sorption sites homogeneously distributed over the sorbent surface and that these sites also have equal affinity for the adsorbate [51]. Furthermore, it is estimated that the surface effects given by the modification with KOH have positively influenced the affinity between the adsorbate and the adsorbent [52].

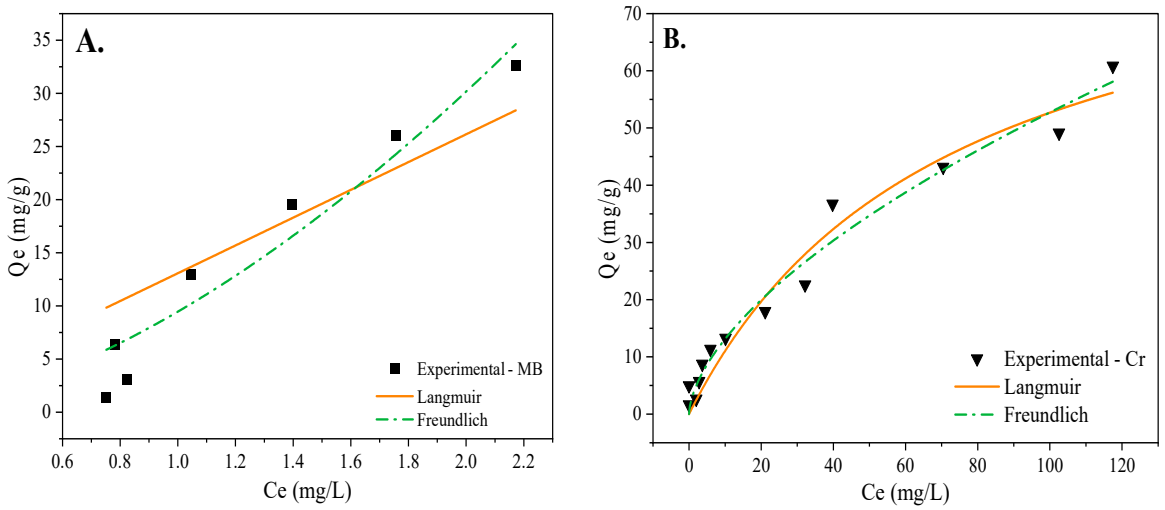



**Figure 10.** Adsorption isotherms of (**A**) MB and (**B**) Cr (VI) using MWBC.

**Table 4.** MB and Cr (VI) adjustment isotherm parameters.

| Model | Parameters | MWBC—MB | MWBC—Cr (VI) |
|---|---|---|---|
| Langmuir | $q_{max}^{L}$ | 186,375.375 | 90.723 |
| | $K_L$ | $7.015 \times 10^{-5}$ | $1.385 \times 10^{-2}$ |
| | $R^2$ | 0.756 | 0.959 |
| Freundlich | $K_F$ | 9.460 | 3.2698 |
| | $n$ | 0.598 | 1.6562 |
| | $R^2$ | 0.918 | 0.969 |

Considering Figure 11A and Table 5, it is evidenced that the MB adsorption kinetic is described by the pseudo-second-order model and Elovich. The above indicates that the process is controlled by physisorption, where the adsorption rate of the dye is proportional to the available sites on the adsorbent, and the reaction rate depends on the amount of dye on the adsorbent surface. Furthermore, there is a coexisting chemisorption mechanism, where the adsorption rate of the dye will decrease exponentially as the amount of dye adsorbed increases [53]. On the other hand, Cr (VI) kinetic was adjusted by Elovich's model, indicating that the process occurs by chemisorption involving electrostatic interaction and ionic exchange between the adsorbate and adsorbent [54,55].

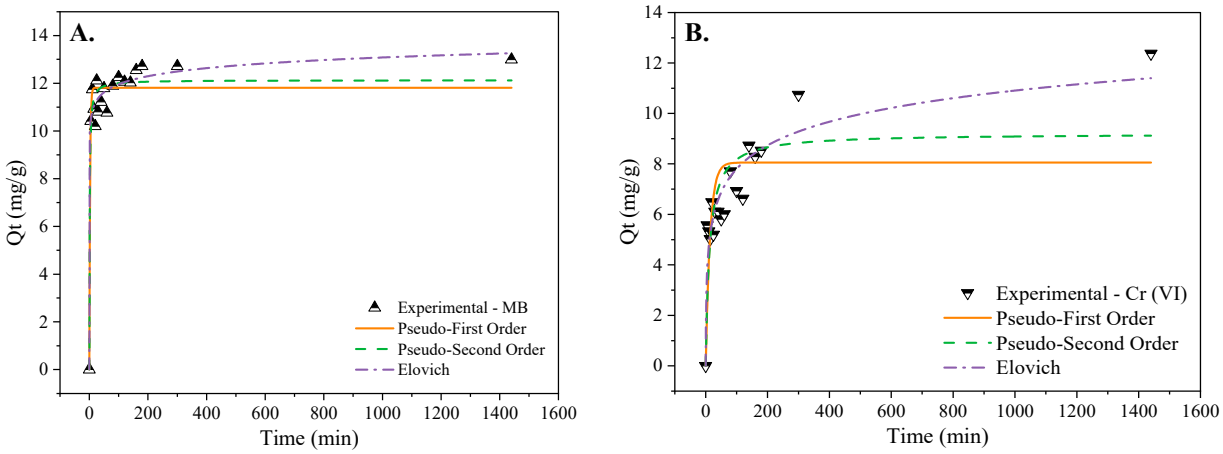



**Figure 11.** (**A**) MB and (**B**) Cr (VI) kinetic modeling onto MWBC.

**Table 5.** MB and Cr (VI) kinetic adjustment parameters.

| Model | Parameter | MWBC—MB | MWBC—Cr (VI) |
|---|---|---|---|
| Pseudo-first order | $q_e$ | 11.812 | 8.05363 |
| | $K_1$ | 0.424 | 0.07054 |
| | $R^2$ | 0.926 | 0.49151 |
| Pseudo-second order | $q_e$ | 12.129 | 9.20214 |
| | $K_2$ | 0.078 | 0.00865 |
| | $R^2$ | 0.945 | 0.66108 |
| Elovich | $\alpha$ | $2.172 \times 10^{8}$ | 4.3733 |
| | $\beta$ | 2.050 | 0.74117 |
| | $R^2$ | 0.967 | 0.87572 |

### *3.4. Competitive Adsorption Tests*

Multicomponent assays (Figure 12) show that the adsorption of MB is not affected by the presence of Cr (VI), and no notable changes are observed when varying the concentration of the interfering metal. Nevertheless, Cr (VI) adsorption is favored by the presence of MB in the system (Figure 12A). It can be said that the MWBC has selectivity towards Cr (VI) when they coexist in an aqueous solution.

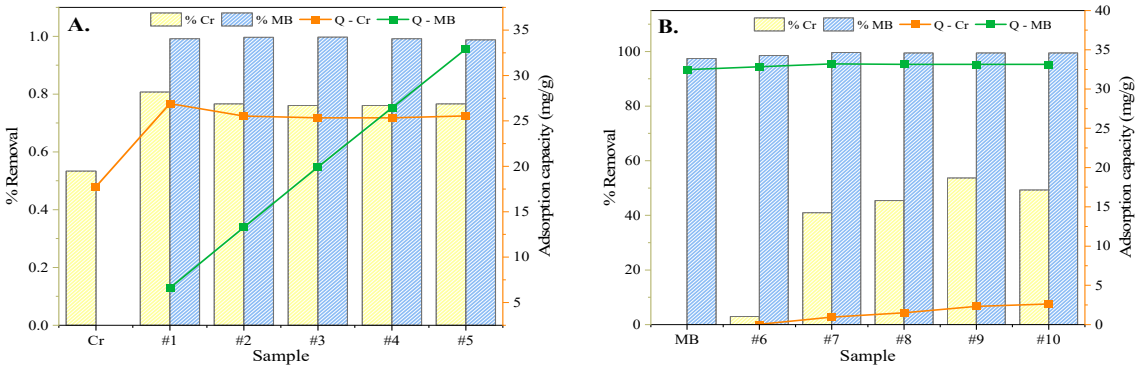



**Figure 12.** Competitive adsorption of MB and chromium when (**A**) Cr (VI) is fixed and (**B**) MB is fixed.

The results of this study can be compared with other investigations that focus on the preparation of biochar for the removal of metals and dyes in solutions. In particular, the results of our study are presented and contrasted with those reported in the literature on marketable biochar in Table 6. This comparison allows us to evaluate the performance of our biochar concerning other materials on the market.

**Table 6.** Comparison of MWBC with commercial biochar.

| Material | Synthesis Parameters | Adsorption Capacity (% Efficiency) | References |
|---|---|---|---|
| Commercial activated carbon | Temperature: 200 °C<br>Time: 45 min<br>Activator: KHO 1:1 | MB: 99 ± 0.5<br>Pb (II): 99 ± 0.5<br>Cd (II): 99 ± 0.4<br>In 12 h | [56] |
| | Temperature: 550 °C<br>Time: 1 h<br>Activator: KOH (1 M y 3 M) | Cr (VI): 87 ± 5<br>in 60 min | [57] |
| MWBC | Temperature: 200 °C<br>Time: 30 min<br>Activator: KOH 3 M | MB: 98.94<br>Cr (VI): 85.15<br>In 24 h | Present study |

These results indicate that the prepared MWBC is a promising adsorbent material for the remediation of water contaminated with cationic dyes and heavy metals. In addition, its selectivity towards MB and Cr (VI) adsorption is highlighted.

## 4. Conclusions

The high efficiency of the MWBC in the adsorption processes of methylene blue and Cr (VI) is presented, demonstrating that thermally treated biomaterials from lignocellulosic waste can replace commercial activated carbon. From SEM analysis, it was evidenced that the formation of tubular cavities and porous structure was caused by the basic hydrolysis with KOH. From adsorption tests, an adsorption capacity of 12.98 mg/g and 97.38% of efficiency was registered for MB at pH 10, while for Cr (VI), it was 11.35 mg/g and 85.15%

at pH 2. Freundlich's model adjusted the adsorption equilibrium data with $R^2 > 0.9$; then, it can be said that the process is controlled by chemisorption. The maximum adsorption capacities in the monolayer were 186.375 mg/g and 90.723 mg/g for Cr (VI) and MB, according to Langmuir's model. From the kinetic study, it can be said that the process occurs by chemisorption through electrostatic interaction and ionic interchange between adsorbate and adsorbent.

**Author Contributions:** Conceptualization, C.T.-T., Á.V.-O. and R.O.-T.; data curation, R.O.-T.; formal analysis, C.T.-T. and Á.V.-O.; methodology, C.T.-T.; project administration, C.T.-T. and Á.V.-O.; resources, C.T.-T. and Á.V.-O.; software, Á.V.-O.; supervision, C.T.-T. and Á.V.-O.; validation, C.T.-T. and R.O.-T.; visualization, R.O.-T.; writing—original draft, Á.V.-O.; writing—review and editing, Á.V.-O. and R.O.-T. All authors have read and agreed to the published version of the manuscript.

**Funding:** This research received no external funding.

**Institutional Review Board Statement:** Not applicable.

**Informed Consent Statement:** Not applicable.

**Data Availability Statement:** The data supporting this study's results are available upon request from the corresponding author.

**Acknowledgments:** The authors thank the Universidad de Cartagena (Colombia) for the support in the development of this work regarding laboratory, software use, and time for their researchers.

**Conflicts of Interest:** The authors declare no conflict of interest.

## References

1. Rangabhashiyam, S.; Balasubramanian, P. Adsorption behaviors of hazardous methylene blue and hexavalent chromium on novel materials derived from *Pterospermum acerifolium* shells. *J. Mol. Liq.* **2018**, *254*, 433–445. [CrossRef]
2. Afshin, S.; Rashtbari, Y.; Shirmardi, M.; Vosoughi, M.; Hamzehzadeh, A. Adsorption of Basic Violet 16 dye from aqueous solution onto mucilaginous seeds of *Salvia sclarea*: Kinetics and isotherms studies. *Desalin. Water Treat.* **2019**, *161*, 365–375. [CrossRef]
3. Li, L.; Liu, F.; Duan, H.; Wang, X.; Li, J.; Wang, Y.; Luo, C. The preparation of novel adsorbent materials with efficient adsorption performance for both chromium and methylene blue. *Colloids Surf. B Biointerfaces* **2016**, *141*, 253–259. [CrossRef]
4. Dinh, V.P.; Huynh, T.D.T.; Le, H.M.; Nguyen, V.D.; Dao, V.A.; Hung, N.Q.; Tuyen, L.A.; Lee, S.; Yi, J.; Nguyen, T.D.; et al. Insight into the adsorption mechanisms of methylene blue and chromium(iii) from aqueous solution onto pomelo fruit peel. *RSC Adv.* **2019**, *9*, 25847–25860. [CrossRef]
5. Diaconu, M.; Pavel, L.V.; Hlihor, R.M.; Rosca, M.; Fertu, D.I.; Lenz, M.; Corvini, P.X.; Gavrilescu, M. Characterization of heavy metal toxicity in some plants and microorganisms—A preliminary approach for environmental bioremediation. *N. Biotechnol.* **2020**, *56*, 130–139. [CrossRef]
6. Iqbal, F.; Ayub, Q.; Wilson, R.; Song, B.K.; Talei, A.; Yeong, K.Y.; Hermawan, A.; Fahim, M.; Rahman, S. Monitoring of heavy metal pollution in urban and rural environments across Pakistan using House crows (*Corvus splendens*) as bioindicator. *Environ. Monit. Assess.* **2021**, *193*, 237. [CrossRef] [PubMed]
7. Geng, J.; Yin, Y.; Liang, Q.; Zhu, Z.; Luo, H. Polyethyleneimine cross-linked graphene oxide for removing hazardous hexavalent chromium: Adsorption performance and mechanism. *Chem. Eng. J.* **2019**, *361*, 1497–1510. [CrossRef]
8. Velusamy, S.; Roy, A.; Sundaram, S.; Kumar Mallick, T. A Review on Heavy Metal Ions and Containing Dyes Removal Through Graphene Oxide-Based Adsorption Strategies for Textile Wastewater Treatment. *Chem. Rec.* **2021**, *21*, 1570–1610. [CrossRef]
9. De Sousa, C.M.; Cardoso, V.L.; Batista, F.R.X. A coupled photocatalytic system using niobium oxide and microalga: Cr (VI)-contaminated wastewater treatment. *J. Photochem. Photobiol. A Chem.* **2023**, *439*, 114602. [CrossRef]
10. Banerjee, S.; Kamila, B.; Barman, S.; Joshi, S.R.; Mandal, T.; Halder, G. Interlining Cr(VI) remediation mechanism by a novel bacterium *Pseudomonas brenneri* isolated from coalmine wastewater. *J. Environ. Manag.* **2019**, *233*, 271–282. [CrossRef]
11. Jiang, Y.; Martinez-Guerra, E.; Gnaneswar Gude, V.; Magbanua, B.; Truax, D.D.; Martin, J.L. Wetlands for Wastewater Treatment. *Water Environ. Res.* **2016**, *88*, 1160–1191. [CrossRef] [PubMed]
12. Magoling, B.J.A.; Macalalad, A.A. Optimization and Response Surface Modelling of Activated Carbon Production from Mahogany Fruit Husk for Removal of Chromium (VI) from Aqueous Solution. *BioResources* **2017**, *12*, 3001–3016. Available online: https://jtatm.textiles.ncsu.edu/index.php/BioRes/article/view/BioRes_12_2_3001_Magoling_Optimization_Response_Surface_Modelling_Fruit_Husk (accessed on 10 June 2023). [CrossRef]
13. Khalil, U.; Shakoor, M.B.; Ali, S.; Rizwan, M.; Alyemeni, M.N.; Wijaya, L. Adsorption-reduction performance of tea waste and rice husk biochars for Cr(VI) elimination from wastewater. *J. Saudi Chem. Soc.* **2020**, *24*, 799–810. [CrossRef]
14. Shakya, A.; Agarwal, T. Removal of Cr(VI) from water using pineapple peel derived biochars: Adsorption potential and re-usability assessment. *J. Mol. Liq.* **2019**, *293*, 111497. [CrossRef]

15. Al-Mokhalelati, K.; Al-Bakri, I.; Wattar, N.A.S.A. Adsorption of methylene blue onto sugarcane bagasse-based adsorbent materials. *J. Phys. Org. Chem.* **2021**, *34*, e4193. [CrossRef]
16. Chen, J.; Yang, J.; Hu, G.; Hu, X.; Li, Z.; Shen, S.; Radosz, M.; Fan, M. Enhanced $CO_2$ Capture Capacity of Nitrogen-Doped Biomass-Derived Porous Carbons. *ACS Sustain. Chem. Eng.* **2016**, *4*, 1439–1445. [CrossRef]
17. Liu, P.; Liu, W.J.; Jiang, H.; Chen, J.J.; Li, W.W.; Yu, H.Q. Modification of bio-char derived from fast pyrolysis of biomass and its application in removal of tetracycline from aqueous solution. *Bioresour. Technol.* **2012**, *121*, 235–240. [CrossRef] [PubMed]
18. Guy, M.; Mathieu, M.; Anastopoulos, I.P.; Martínez, M.G.; Rousseau, F.; Dotto, G.L.; de Oliveira, H.P.; Lima, E.C.; Thyrel, M.; Larsson, S.H.; et al. Process Parameters Optimization, Characterization, and Application of KOH-Activated Norway Spruce Bark Graphitic Biochars for Efficient Azo Dye Adsorption. *Molecules* **2022**, *27*, 456. [CrossRef]
19. Kaya, N.; Uzun, Z.Y. Investigation of effectiveness of pine cone biochar activated with KOH for methyl orange adsorption and $CO_2$ capture. *Biomass Convers. Biorefinery* **2020**, *11*, 1067–1083. [CrossRef]
20. Goertzen, S.L.; Thériault, K.D.; Oickle, A.M.; Tarasuk, A.C.; Andreas, H.A. Standardization of the Boehm titration. Part I. $CO_2$ expulsion and endpoint determination. *Carbon* **2010**, *48*, 1252–1261. [CrossRef]
21. Alberto, F.; Villa, A.; Anaguano, A.H. Determinación del punto de carga cero y punto isoeléctrico de dos residuos agrícolas y su aplicación en la remoción de colorantes. *RIAA* **2013**, *4*, 27–36. Available online: https://dialnet.unirioja.es/servlet/articulo?codigo=5344979&info=resumen&idioma=ENG (accessed on 10 June 2023).
22. *ASTM C1777-20*; Standard Test Method for Rapid Determination of the Methylene Blue Value for Fine Aggregate or Mineral Filler Using a Colorimeter. ASTM International: West Conshohocken, PA, USA, 2020. Available online: https://www.astm.org/c1777-20.html (accessed on 10 June 2023).
23. Liu, X.J.; Li, M.F.; Singh, S.K. Manganese-modified lignin biochar as adsorbent for removal of methylene blue. *J. Mater. Res. Technol.* **2021**, *12*, 1434–1445. [CrossRef]
24. Somsesta, N.; Piyamawadee, C.; Sricharoenchaikul, V.; Aht-Ong, D. Adsorption isotherms and kinetics for the removal of cationic dye by Cellulose-based adsorbent biocomposite films. *Korean J. Chem. Eng.* **2020**, *37*, 1999–2010. [CrossRef]
25. Altun, T.; Pehlivan, E. Removal of Cr(VI) from aqueous solutions by modified walnut shells. *Food Chem.* **2012**, *132*, 693–700. [CrossRef]
26. *ASTM D1687-17*; Standard Test Methods for Chromium in Water. ASTM International: West Conshohocken, PA, USA, 2017. Available online: https://www.astm.org/d1687-17.html (accessed on 12 June 2023).
27. Patel, H. Comparison of batch and fixed bed column adsorption: A critical review. *Int. J. Environ. Sci. Technol.* **2021**, *19*, 10409–10426. [CrossRef]
28. Ul-Islam, S. *Advanced Materials for Wastewater Treatment*; Wiley: Hoboken, NJ, USA, 2017; ISBN 978-1-119-40780-5.
29. Al-Ghouti, M.A.; Da'ana, D.A. Guidelines for the use and interpretation of adsorption isotherm models: A review. *J. Hazard. Mater.* **2020**, *393*, 122383. [CrossRef]
30. Zhang, J.; Zhang, P.; Zhang, S.; Zhou, Q. Comparative Study on the Adsorption of Tartrazine and Indigo Carmine onto Maize Cob Carbon. *Sep. Sci. Technol.* **2014**, *49*, 877–886. [CrossRef]
31. Edet, U.A.; Ifelebuegu, A.O. Kinetics, Isotherms, and Thermodynamic Modeling of the Adsorption of Phosphates from Model Wastewater Using Recycled Brick Waste. *Processes* **2020**, *8*, 665. [CrossRef]
32. Wang, J.; Guo, X. Adsorption kinetic models: Physical meanings, applications, and solving methods. *J. Hazard. Mater.* **2020**, *390*, 122156. [CrossRef]
33. Qu, J.; Wang, Y.; Tian, X.; Jiang, Z.; Deng, F.; Tao, Y.; Jiang, Q.; Wang, L.; Zhang, Y. KOH-activated porous biochar with high specific surface area for adsorptive removal of chromium (VI) and naphthalene from water: Affecting factors, mechanisms and reusability exploration. *J. Hazard. Mater.* **2021**, *401*, 123292. [CrossRef]
34. Aigbe, U.O.; Osibote, O.A. Carbon derived nanomaterials for the sorption of heavy metals from aqueous solution: A review. *Environ. Nanotechnol. Monit. Manag.* **2021**, *16*, 100578. [CrossRef]
35. Rodríguez, A.; Ovejero, G.; Sotelo, J.L.; Mestanza, M.; García, J. Adsorption of dyes on carbon nanomaterials from aqueous solutions. *J. Environ. Sci. Health Part A* **2010**, *45*, 1642–1653. [CrossRef] [PubMed]
36. Borba, L.L.; Cuba, R.M.F.; Cuba Terán, F.J.; Castro, M.N.; Mendes, T.A. Use of adsorbent biochar from pequi (Caryocar Brasiliense) husks for the removal of commercial formulation of glyphosate from aqueous media. *Braz. Arch. Biol. Technol.* **2019**, *62*, e19180450. [CrossRef]
37. Labied, R.; Physico-chimiques, A.; Oumessaad Benturki, A.; Poincaré-Nancy, H.I. Adsorption of hexavalent chromium by activated carbon obtained from a waste lignocellulosic material (*Ziziphus jujuba* cores): Kinetic, equilibrium, and thermodynamic study Adh' Ya Eddine Hamitouche André Donnot. *Adsorpt. Sci. Technol.* **2018**, *36*, 1066–1099. [CrossRef]
38. Suhaimi, N.; Kooh, M.R.R.; Lim, C.M.; Chou Chao, C.T.; Chou Chau, Y.F.; Mahadi, A.H.; Chiang, H.P.; Haji Hassan, N.H.; Thotagamuge, R. The Use of Gigantochloa Bamboo-Derived Biochar for the Removal of Methylene Blue from Aqueous Solution. *Adsorpt. Sci. Technol.* **2022**, *2022*, 8245797. [CrossRef]
39. Siqueira, C.; da Silva, I.; Rubio, A.; Bergamasco, R.; Gasparotto, F.; Paccola, E.; Yamaguchi, N. Sugarcane Bagasse as an Efficient Biosorbent for Methylene Blue Removal: Kinetics, Isotherms and Thermodynamics. *Int. J. Environ. Res. Public Health* **2020**, *17*, 526. [CrossRef] [PubMed]
40. Gaffney, J.S.; Marley, N.A.; Jones, D.E. Fourier Transform Infrared (FTIR) Spectroscopy. In *Characterization of Materials*; John Wiley & Sons, Inc.: Hoboken, NJ, USA, 2012; pp. 1–33. [CrossRef]

41. Grams, J. Surface analysis of solid products of thermal treatment of lignocellulosic biomass. *J. Anal. Appl. Pyrolysis* **2022**, *161*, 105429. [CrossRef]
42. Park, D.; Yun, Y.S.; Jong, M.P. Studies on hexavalent chromium biosorption by chemically-treated biomass of *Ecklonia* sp. *Chemosphere* **2005**, *60*, 1356–1364. [CrossRef]
43. Seung Kim, Y.; Rae Park, C. Titration Method for the Identification of Surface Functional Groups. In *Materials Science and Engineering of Carbon: Characterization*; Butterworth-Heinemann: Oxford, UK, 2016; pp. 273–286. ISBN 9780128052563.
44. Titchou, F.E.; Zazou, H.; Afanga, H.; El Gaayda, J.; Akbour, R.A.; Hamdani, M. Removal of Persistent Organic Pollutants (POPs) from water and wastewater by adsorption and electrocoagulation process. *Groundw. Sustain. Dev.* **2021**, *13*, 100575. [CrossRef]
45. Yagub, M.T.; Sen, T.K.; Afroze, S.; Ang, H.M. Dye and its removal from aqueous solution by adsorption: A review. *Adv. Colloid Interface Sci.* **2014**, *209*, 172–184. [CrossRef]
46. Rakhunde, R.; Deshpande, L.; Juneja, H.D. Chemical Speciation of Chromium in Water: A Review. *Crit. Rev. Environ. Sci. Technol.* **2012**, *42*, 776–810. [CrossRef]
47. Lian, G.; Wang, B.; Lee, X.; Li, L.; Liu, T.; Lyu, W. Enhanced removal of hexavalent chromium by engineered biochar composite fabricated from phosphogypsum and distillers grains. *Sci. Total Environ.* **2019**, *697*, 134119. [CrossRef]
48. Nguyen, T.A.H.; Ngo, H.H.; Guo, W.S.; Zhang, J.; Liang, S.; Yue, Q.Y.; Li, Q.; Nguyen, T.V. Applicability of agricultural waste and by-products for adsorptive removal of heavy metals from wastewater. *Bioresour. Technol.* **2013**, *148*, 574–585. [CrossRef] [PubMed]
49. Soliman, N.K.; Moustafa, A.F. Industrial solid waste for heavy metals adsorption features and challenges; a review. *J. Mater. Res. Technol.* **2020**, *9*, 10235–10253. [CrossRef]
50. Zhou, L.; Liu, Y.; Liu, S.; Yin, Y.; Zeng, G.; Tan, X.; Hu, X.; Hu, X.; Jiang, L.; Ding, Y.; et al. Investigation of the adsorption-reduction mechanisms of hexavalent chromium by ramie biochars of different pyrolytic temperatures. *Bioresour. Technol.* **2016**, *218*, 351–359. [CrossRef] [PubMed]
51. Choudhary, B.; Paul, D. Isotherms, kinetics and thermodynamics of hexavalent chromium removal using biochar. *J. Environ. Chem. Eng.* **2018**, *6*, 2335–2343. [CrossRef]
52. Tytłak, A.; Oleszczuk, P.; Dobrowolski, R. Sorption and desorption of Cr(VI) ions from water by biochars in different environmental conditions. *Environ. Sci. Pollut. Res.* **2014**, *22*, 5985–5994. [CrossRef] [PubMed]
53. William Kajjumba, G.; Emik, S.; Öngen, A.; Kurtulus Özcan, H.; Aydın, S. Modelling of Adsorption Kinetic Processes—Errors, Theory and Application. In *Advanced Sorption Process Applications*; IntechOpen: London, UK, 2019; pp. 187–198. ISBN 978-1-78984-819-9. [CrossRef]
54. Amaku, J.F.; Ngwu, C.M.; Nnaji, J.C.; Odoemelam, S.A.; Ifeanyi, U.B.; Okorie, H.; Zubairu, S.M. Adsorption of Cr(VI) onto *Azadirachta indica* stem bark extract modified dolerite composite adsorbent. *Int. J. Environ. Anal. Chem.* **2021**. [CrossRef]
55. Villabona-Ortíz, A.; Tejada-Tovar, C.N.; Ortega-Toro, R. Modelling of the adsorption kinetics of chromium (VI) using waste biomaterials. *Rev. Mex. Ing. Química* **2020**, *19*, 401–408. [CrossRef]
56. Sherugar, P.; Padaki, M.; Naik, N.S.; George, S.D.; Murthy, D.H.K. Biomass-derived versatile activated carbon removes both heavy metals and dye molecules from wastewater with near-unity efficiency: Mechanism and kinetics. *Chemosphere* **2022**, *287*, 132085. [CrossRef]
57. Jamil, U.; Zeeshan, M.; Khan, S.R.; Saeed, S. Synthesis and two-step KOH based activation of porous biochar of wheat straw and waste tire for adsorptive exclusion of chromium (VI) from aqueous solution: Thermodynamic and regeneration study. *J. Water Process Eng.* **2023**, *53*, 103892. [CrossRef]


**Disclaimer/Publisher's Note:** The statements, opinions and data contained in all publications are solely those of the individual author(s) and contributor(s) and not of MDPI and/or the editor(s). MDPI and/or the editor(s) disclaim responsibility for any injury to people or property resulting from any ideas, methods, instructions or products referred to in the content.